JOURNAL OF GEOPHYSICAL RESEARCH, VOL. 102, NO. C13, PAGES 27,813–27,824, DECEMBER 15, 1997

Annual cycle of sea surface temperature in the tropical Atlantic Ocean

James A. Carton and Zengxi Zhou[1]
Department of Meteorology, University of Maryland, College Park

Abstract. The strongest temporal variation of sea surface temperature (SST) in the Atlantic occurs at the annual period. In this paper we examine the causes of the annual cycle of SST through a series of modeling studies. In the subtropics we find that the annual cycle of SST follows the annual cycle of net shortwave radiation, except near the eastern boundary. Off northwest Africa, the annual cycle results from coastal upwelling induced by annual variations in alongshore winds. Off southwest Africa, the annual cycle results from a combination of coastal upwelling and effects caused by changes in the trade winds along the equator. In the band of latitudes between 3°N and 10°N, changes in latent heat loss due to the annual variation in wind speed is most important. The dominance of latent heat loss in this region explains why SST reaches a maximum in boreal fall even though the depth of the thermocline is at its annual minimum.

1. Introduction

Despite many studies of the annual cycle of currents and heat storage in the tropical and subtropical Atlantic [e.g., *Garzoli and Katz*, 1983; *Busalacchi and Picaut*, 1983; *Merle and Arnault*, 1985; *du Penhoat and Triguier*, 1985; *Philander and Pacanowski*, 1986], little is yet known about the causes of the annual cycle of sea surface temperature (SST). This is surprising because SST is the most important physical parameter of the ocean affecting the atmosphere. Similar to the eastern Pacific, the variability of SST in the tropical Atlantic is concentrated at the annual period (Figure 1). At high latitudes the annual SST cycle results from heating in the summer by solar radiation and cooling in the fall and winter due to mixing and radiative heat loss. In the subtropics, mixing effects become less important. Along the equator the annual cycle results mainly from zonal shifts of heat. In this paper we investigate the extent of these dynamic and thermodynamic regimes through a series of numerical simulations with a general circulation model of the ocean.

The seasonal cycle of the tropical Atlantic shares a number of similarities with the eastern Pacific, including strong annually varying trade winds and the appearance in boreal fall of a cold tongue of SST extending westward from the coast. Because of the similarities between the oceans and the absence of studies of Atlantic SST, we begin with a review of studies of the seasonal cycle of SST in the tropical Pacific. One of the first such studies was *Wyrtki*'s [1981] examination of the surface heat budget. Based on a limited observational record, Wyrtki concluded that surface heat flux, zonal temperature advection, and upwelling were all important in regulating SST change. This approach was revisited by *Hayes et al.* [1991] using the more extensive data of the Tropical Ocean/Global Atmosphere Tropical Atmosphere-Ocean (TAO) mooring array. Hayes et al. also found no dominant balance in the SST equation. However, they found that the largest terms in the eastern Pacific were net surface heat flux and net heat loss through the base of the mixed layer.

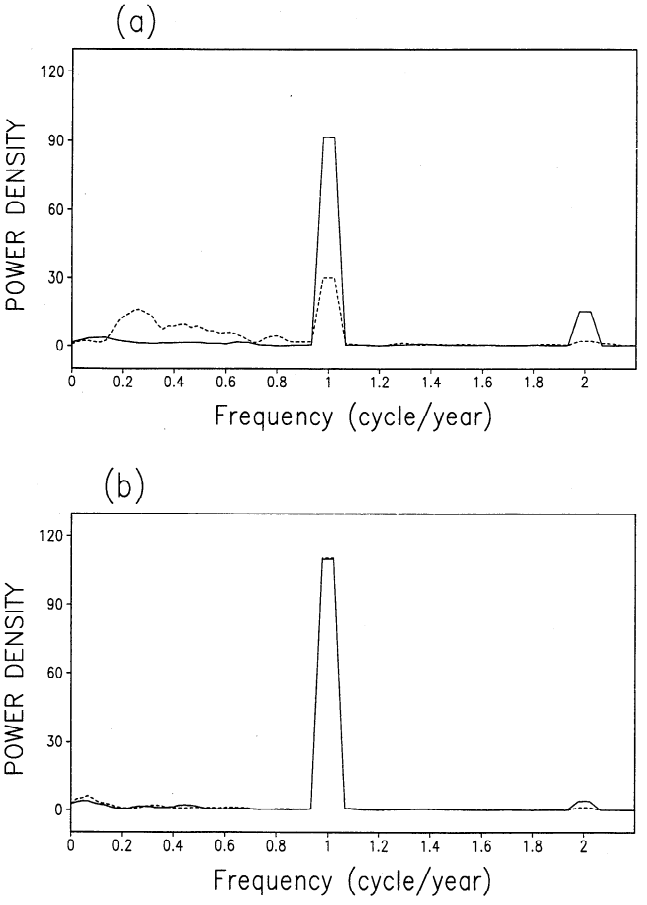

Figure 1. (a) Normalized power spectra of SST in Atlantic (0°N, 20°W, solid curve) and eastern Pacific (0°N, 140°W, dashed curve). (b) Similar to Figure 1a but at 20°N. The spectra are normalized by the variance of time series.

[1]Currently at the Atlantic Oceanographic Marine Laboratory, NOAA, Miami, Florida.

Paper number 97JC02197.
0148-0227/97/97JC-02197$09.00

Table 1. Model Experiments

Experiment	Forcing Fields
Control	monthly τ, S_W, L_W, Q_E, and Q_S
1	annual mean S_W
2	annual mean U_a in Q_E
3	annual mean γ in Q_E
4	annual mean τ
5	annual mean τ^x
6	annual mean τ^y
7	annual mean $\tau(x < 28°\text{W})$

Each experiment is similar to the control run except for the modification indicated.

A series of modeling studies have been conducted to examine the annual cycle of SST in the eastern Pacific [e.g., *Seager et al.*, 1988; *Harrison*, 1991]. In each of these studies a model was developed that could simulate the observed annual cycle of SST. Then an effort was made to estimate the size of different terms in the mixed layer heat budget. Harrison applied this approach to a general circulation model but with (in our opinion) an excessively crude parameterization of surface heat flux. He concluded that the dominant terms in the mixed layer heat budget in the eastern Pacific were the warming effects of meridional advection and the cooling effects of upwelling. Seager et al. introduced a much simpler $1\frac{1}{2}$ layer model but with an improved parameterization of surface heat flux. They found that surface heating altered SST by reducing near-surface mixing, thus reducing heat loss at the base of the mixed layer. Two additional studies by *Giese and Cayan* [1993] and *Koberle and Philander* [1994] provided a more extensive analysis of the behavior of the general circulation model. One of the interesting results of the latter study was the recognition of the role of surface heating in altering SST indirectly by reducing near-surface mixing, and thus reducing the heat loss at the base of the mixed layer. This mechanism, originally proposed by *Kraus* [1977], enhances the direct effect of surface heating on the mixed layer temperture.

In the modeling studies described above, little attempt has been made to account for the coupled interaction that allows semiannual variations in solar radiation to produce annual variations in winds, heating, and SST. Recently, observational studies by *Mitchell and Wallace* [1992], *Wang* [1994], and *Nigam and Chao* [1997] have suggested a conceptual picture of how this occurs in the Pacific. The initiation mechanism accepted by all three studies is essentially terrestrial. In boreal summer, differential heating of the American continental land mass causes northward monsoonal flow near the eastern boundary of the Pacific. The southern hemisphere experiences strong coastal upwelling and low SST as a result. Thus in boreal summer, SST is asymmetric about the equator. In austral summer the coastal winds do not produce strong upwelling in the northern coastal zone. Also in austral summer, coastal waters in both hemispheres remain warm because neither hemisphere is cooled by upwelling.

Nigam and Chao [1997] suggest that the asymmetry of SST at the coast of South America propagates westward in the Pacific through local interaction between zonal winds and SST. In boreal summer, cold water near the southern coast sets up an eastward gradient of atmospheric boundary layer pressure, enhancing easterly zonal winds. The intensified easterly winds cool equatorial SST either through enhanced upwelling, as the authors suggest, or through increased latent heat release. Either process acts to expand the region of cool water by continually shifting the zone of SST gradient toward the west. When the coastal winds reverse direction, upwelling halts, and an expanding zone of warm water emanates from the coast.

In this paper we attempt to extend some of the ideas developed to explain the annual cycle in the Pacific to the case of the Atlantic. The geometry of the eastern boundary in the tropical Atlantic is different from the eastern boundary of the Pacific. An even more important difference between the oceans is the presence of the Amazon basin to the west of the Atlantic and Africa to the east. Atmospheric convection, in particular, strongly influences the intensity of the trade winds. This is because the surface winds are partly controlled by the rate of atmospheric convection occurring in the Amazon basin. Convection in the Amazon basin is itself controlled by interactions with the land surface processes. Thus the presence of neighboring land masses increases the difficulty of constructing a meaningful simple model of surface winds at the annual period. In contrast to winds, surface heat flux is mainly a function of local variables. In this study we do not try to examine the complete coupled system. Instead, we independently specify surface wind stress but model the oceanic and coupled heating processes that control SST.

We begin by carrying out a control integration in which all forcing terms are included. We then conduct a series of experiments designed to examine properties of the annual cycle, beginning with its dependence on surface forcing. In the equations of oceanic motion and the equations for surface heating there are four sources of variability at the annual period. These are (1) net solar heating forced by changes in solar declination, Earth-Sun distance, and cloudiness; (2) evaporative heat loss, forced by changes in surface wind speed and saturation specific and relative humidity; and (3) surface momentum flux, reflecting changes in surface wind stress. We examine the impact of each of these terms by conducting a series of experiments, listed in Table 1, replacing each forcing term with its annual average and then comparing the results with the control run.

2. Model

The ocean model is based on the Geophysical Fluid Dynamics Laboratory Modular Ocean Model code in a domain similar to that of *Philander and Pacanowski* [1986]. The basin domain extends from 30°S to 50°N and from coast to coast. The longitudinal resolution is a constant 1°. Latitudinal resolution is 1/3° between 10°S and 10°N, increasing gradually poleward of this region to 20°. The vertical resolution is 10 m in the upper 100 m, expanding toward the deep ocean for a total of 27 vertical levels. Vertical mixing is Richardson number dependent, following *Pacanowski and Philander* [1981], while horizontal diffusion and viscosity are a constant 2×10^7 cm^2/s. The model is forced with the seasonal cycle of wind stress and solar radiation computed from the Coupled Ocean Atmosphere Data Set (COADS) surface observation data set [*da Silva et al.*, 1994].

Heat flux at the surface can be broken into four terms: net solar radiation, longwave radiation, latent heat loss, and sensible heat loss ($Q = S_W - L_W - Q_E - Q_S$). The annual cycle of COADS net solar radiation, shown in Figure 2b, reaches a maximum of nearly 70 W m^{-2} at ±20° latitude and approaches zero near the equator. In the northern hemisphere, maximum incident solar radiation occurs in July, except off northwest Africa, where it occurs a month or two earlier. The

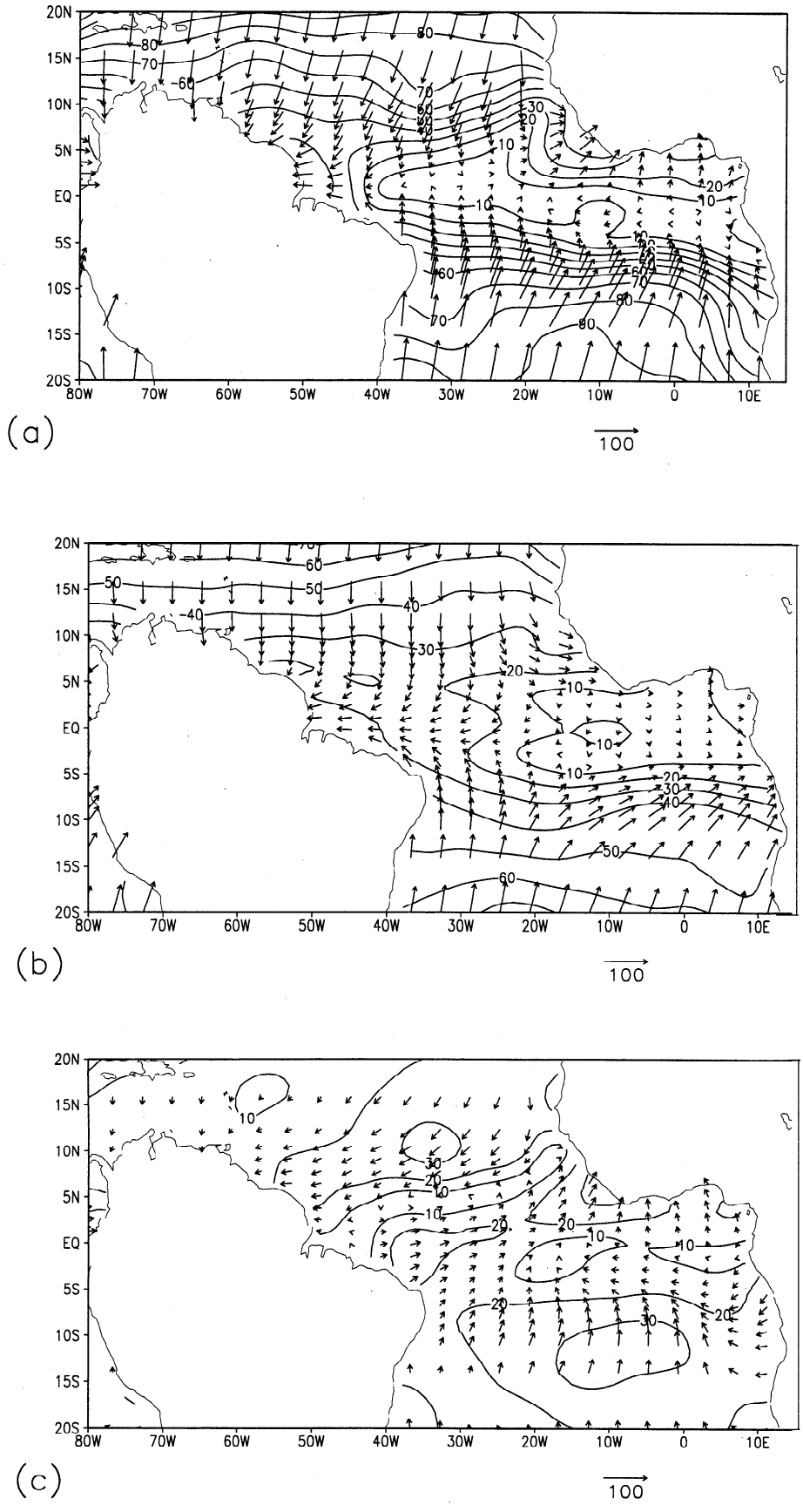

Figure 2. Observed amplitude and phase of the annual cycle of surface heat flux, showing (a) net surface heat flux, (b) net solar radiation, and (c) latent heat flux. Contour interval is 10 W m $^{-2}$. An arrow that is pointing straight up indicates maximum occurs in January. An arrow that is pointing straight down indicates the maximum occurs in July. Phase increases clockwise.

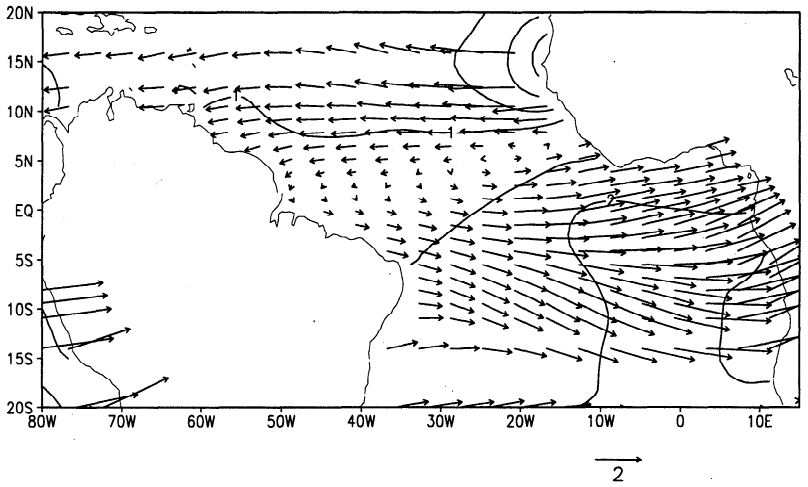

Figure 3. Observed amplitude and phase of SST annual cycle. An arrow that is pointing straight up indicates maximum occurs in January. Phase increases clockwise. Contour interval is 1°C.

reduction in solar radiation in summer in this region is the result of convective clouds. In the southern hemisphere the maximum occurs in January–February, with later phase in broad areas of the eastern basin. The delayed maximum in surface solar radiation in the southern hemisphere is the result of low-level stratus clouds that form in austral summer. The southern hemisphere maximum exceeds the northern hemisphere maximum by about 10%, partly due to the ellipticity of Earth's orbit.

For this simulation, monthly net longwave radiation is parameterized in terms of SST following *Budyko* [1974]. Latent heat loss depends on SST, surface air temperature (SAT), surface pressure p_a, relative humidity γ, saturation vapor pressure e_s, and surface wind speed U_a as

$$Q_E = \rho C_D L |U_a| [e_s(\text{SST}) - \gamma e_s(\text{SAT})](0.622/p_a) \quad (1)$$

The importance of annual variations of relative humidity is examined in experiment 3. In all other experiments, γ is replaced with its annual average.

Ideally, one would like to parameterize surface air temperature in terms of a predicted variable such as SST, as has been done for example, by *Seager et al.* [1995]. However, doing so with a general circulation model may lead to unacceptable systematic temperature drift during long integrations and an unrealistic amplitude of the annual cycle. We adopt a compromise, following *Giese and Cayan* [1993], in which SAT is given by a combination of the observed annual mean air temperature $\overline{\text{SAT}}_{\text{obs}}$, observed annual mean air-sea temperature difference $\overline{\delta T}_{\text{obs}}$, and simulated model SST as $\text{SAT} = \alpha(\text{SST} - \overline{\delta T}_{\text{obs}}) + (1 - \alpha)\overline{\text{SAT}}_{\text{obs}}$. One may interpret this equation as a prediction equation for surface air temperature. Here, after some experimentation, α has been assigned to be 0.75. This large value ensures that the predicted SAT does not depend too much on the specified $\overline{\text{SAT}}_{\text{obs}}$, but at the same time the simulated SST does not develop unacceptable systematic drift. Use of this model avoids inappropriately specifying the annual cycle of SST (which we are studying!). Sensible heat loss is also given as a function of air-sea temperature difference and surface wind speed:

$$Q_S = \rho C_D C_p |U_a| (\text{SST} - \text{SAT}) \quad (2)$$

It is through these two terms, Q_E and Q_S, that air temperature provides negative feedback on simulated SST. In the Q_E term the seasonal change of wind speed cannot be ignored even in equatorial regions. In some regions, observational studies show that the ocean loses much more latent heat in cold seasons than in warm seasons because of this effect [*Liu and Gautier*, 1990]. The model is forced for 5 years with COADS monthly wind stress, solar radiation, and wind speed, starting with January climatological temperature and salinity conditions. The model output beginning in the third year is used to compute the annual harmonic. The model experiments for this study are listed in Table 1. In all the model experiments the same climatological initial conditions of temperature and salinity fields are used.

3. Results

The observed annual cycle of SST has two distinct regions, one north and one south of the thermal equator at approximately 5°N (Figure 3). To the north, SST reaches its peak in September, while to the south the SST reaches its peak in March–April. The largest amplitudes in either hemisphere occur in the east, where the thermocline is shallow. Off northwest and southwest Africa the amplitude of the annual cycle exceeds 3°C. Along the equator, SST follows the annual cycle of the southern hemisphere SST, with maximum temperature in March and minimum temperature in September. The cold water appears first along the equator between 10°W and 0°W and then expands westward. A westward expansion is also apparent in the eastern Pacific cold tongue [*Horel*, 1981]. Further discussion of the annual cycle of SST is provided by *Weingartner and Weisberg* [1991b].

The SST annual cycle for the control run is shown in Figure 4. The major features of the observed annual cycle described above are reproduced, including the change of phase across 5°N (compare Figures 3 and 4). The main deficiencies in the simulated SST are related to errors in vertical mixing, resulting in a mixed layer that is too shallow. This is particularly noticeable in wintertime, when surface cooling and strong wind-induced turbulence should both act to deepen the mixed layer. As a result, at 20°N the control run SST is minimum in early February, a month and a half earlier than observed. The eastern equatorial region north of the equator is another region of

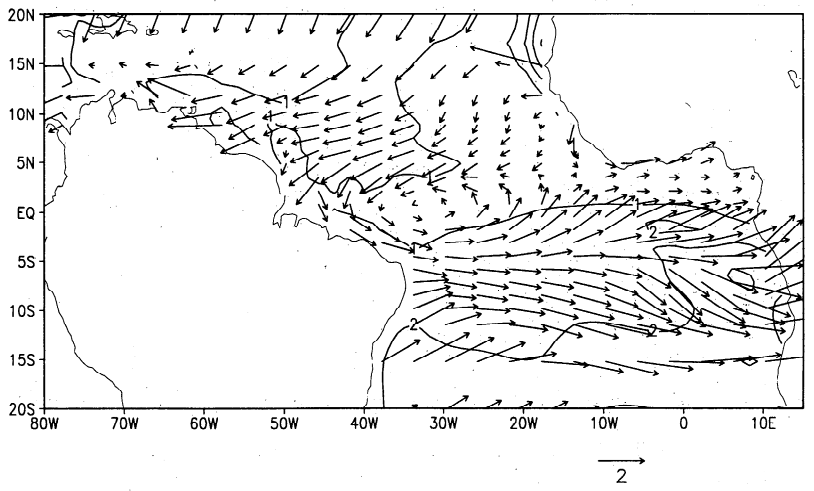

Figure 4. Annual cycle of SST from control run. An arrow that is pointing straight up indicates maximum occurs in January. Phase increases clockwise. Contour interval is 1°C.

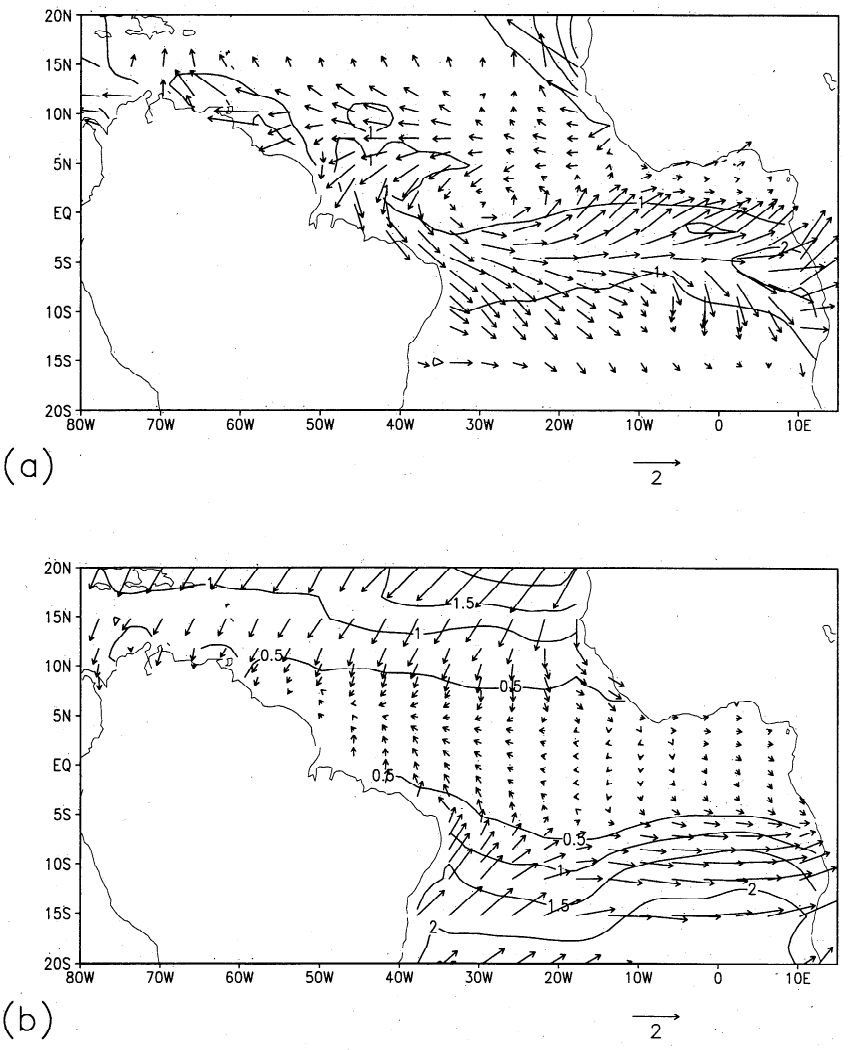

Figure 5. Annual cycle of SST from experiment 1, in which the incident solar radiation is replaced with its climatological annual average. An arrow that is pointing straight up indicates maximum occurs in January. Phase increases clockwise. Figure 5a shows amplitude and phase, and Figure 5b shows amplitude and phase of the difference between control run SST and experiment 1 SST. The difference may be interpreted as the contribution to the annual cycle of SST from the annual cycle of solar radiation. Contour intervals are 1°C and 0.5°C.

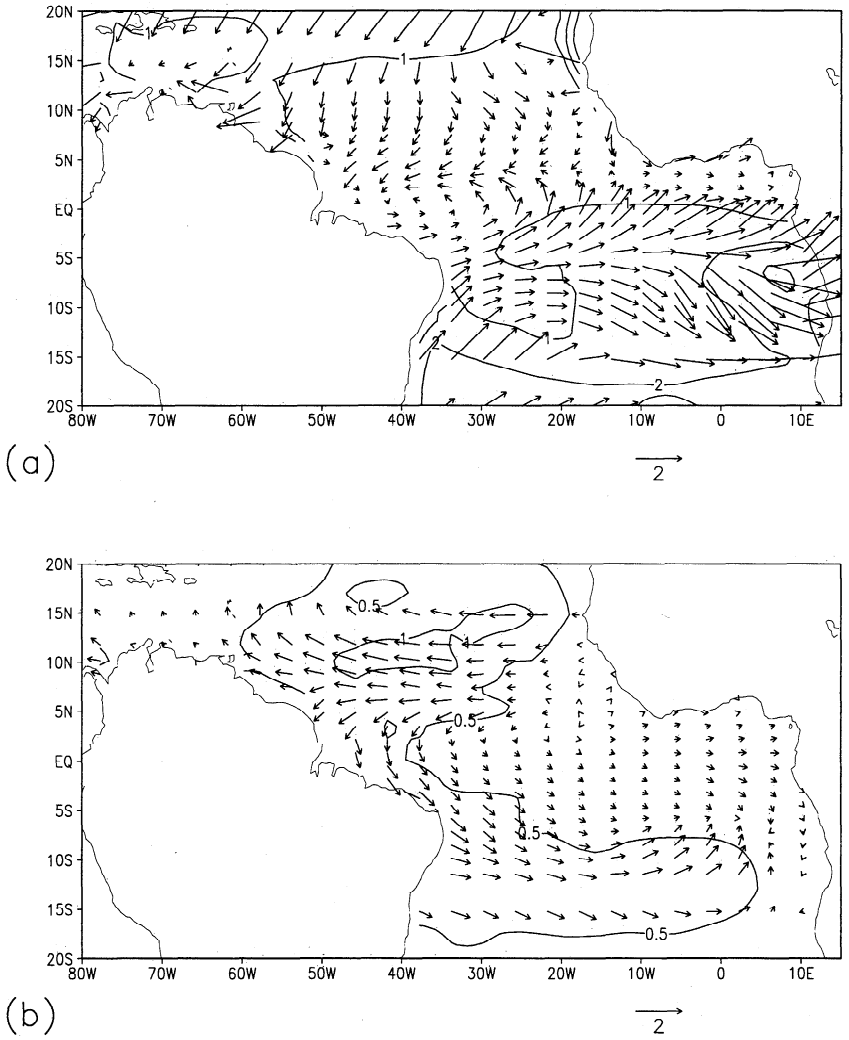

Figure 6. Annual cycle of SST from experiment 2, in which the wind-induced variations in latent heating are replaced with its climatological annual average. An arrow that is pointing straight up indicates maximum occurs in January. Phase increases clockwise. Figure 6a shows amplitude and phase, and Figure 6b shows amplitude and phase of the difference between control run SST and experiment 2 SST. The difference may be interpreted as the contribution to the annual cycle of SST from latent heating variations due to wind variations. Contour intervals are 1°C and 0.5°C.

large errors in the control run. These errors are the result of the fact that the cold tongue in the control run is restricted to the waters south of about 2°N, instead of extending to 4°N. In this location too, errors in vertical mixing may play a role, but errors in surface heating and winds may also be important. The annual variations of simulated current and heat storage are explored by *Philander and Pacanowski* [1986] and *Carton and Hackert* [1990] with a model very similar to the one used in this study.

Through the remainder of this paper we will assume that the physics of the model is approximately correct. We begin by presenting four experiments to find the contribution of each of the four terms in the surface forcing in generating the annual cycle of SST. For each experiment, we focus on the difference from the control run to emphasize the changes.

3.1. Solar Radiation

In the first experiment the control run is repeated with identical initial and surface boundary conditions, with the exception that the seasonal cycle of solar heating is replaced with its annual average. Figure 5b shows the difference between the SST annual cycle of the control run and experiment 1, reflecting the spatially varying impact of solar radiation on the simulation. Solar heating is most important south of 5°S and north of 10°N. The amplitude of the SST annual cycle produced by solar heating increases from 0.3°C in the equatorial region to about 1.2°C at 20°N and 2.4°C at 20°S.

3.2. Wind-Induced Latent Heating

The next term in the annual surface heat budget with important spatial variations (up to 30 W m^{-2}) is latent heat flux. The annual cycle of the latent heat flux reaches its maximum at latitudes of $\pm 10°$, where the contributions of relative humidity and wind speed to the bulk formula for latent heat flux reach their maximum amplitude. In the northern hemisphere the minimum occurs in August at the time when the trade winds there are weakest. In the southern hemisphere the minimum occurs in January, coincident with weakening trade winds at that latitude (Figure 2c). Wind speed and latent heat loss are minimum when solar heating is close to its maximum through-

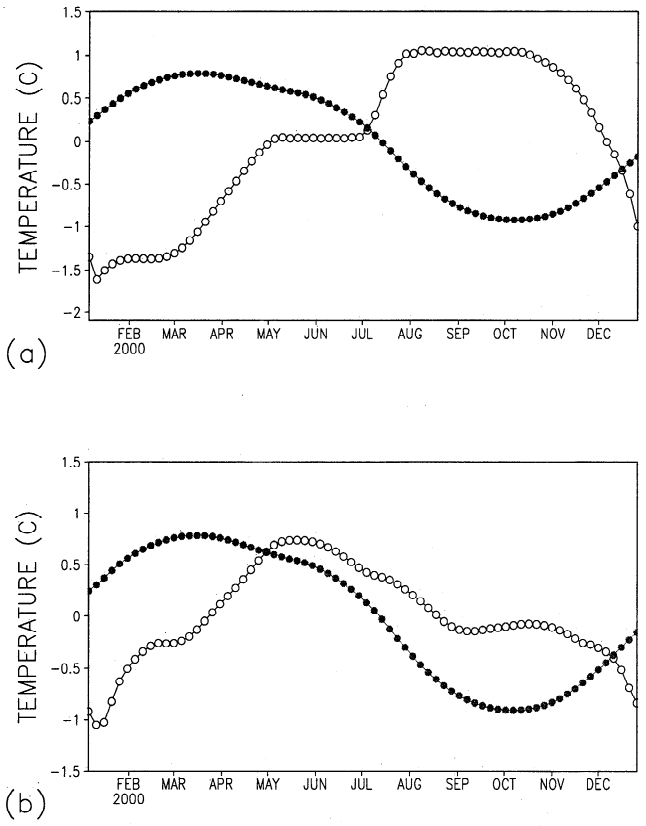

Figure 7. Monthly variations of simulated SST (open circles) and temperature at 100 m depth (solid circles) at 10°N, 40°W. The annual mean has been removed from each time series. Figure 7a shows the control run, and Figure 5b shows experiment 2. Note that SST is warmest in the control run when 100 m temperature is coldest.

out much of the basin. As a result, the amplitude of net heat flux is larger than the amplitude of solar heating over most of the tropical Atlantic.

In experiment 2 the wind speed term in the latent heat flux calculation (1) is replaced with its climatological annual average. It is evident from Figure 6 that wind-induced latent heat flux is an important factor in the band of latitudes 15°S–8°S west of 0°E and also in the area of 5°N–20°N, 55°W–20°W. In some of these regions, wind-induced changes in latent heat flux explain more than half of the annual cycle of SST.

The importance of latent heat flux explains a puzzling observation that is also reproduced by the simulation between 8°N and 13°N (Figure 7). In this band of latitudes the thermocline is deepest in April, at a time when SST is minimum. Similarly, SST is highest when the thermocline is shallowest. The explanation for this counterintuitive result is that in summer as the Intertropical Convergence Zone (ITCZ) shifts northward, Ekman pumping increases and thus the thermocline rises. However, since the winds diminish in the neighborhood of the ITZ, latent heat loss decreases. The change in latent heat loss is so dramatic that SST goes up although both cloudiness and heat loss due to mixing across the thermocline also increase.

3.3. Humidity-Induced Latent Heating

The rate of latent heat loss depends on local humidity as well as wind speed. On interannual timescales the effect may be of considerable importance because of the interannual changes in evaporation over western Africa [*Blumenthal*, 1990]. At the annual period, relative humidity rises to mid-80% values near the ITCZ and drops to 75% or less in the subtropical regions of large-scale descending motion. However, Figure 8 shows that over much of the basin the effect on annual SST is 0.25°C or less. The effect of annually varying humidity is largest off northwest Africa, where an increase in humidity in northern summer causes the waters to warm by 0.5°C.

3.4. Ocean Dynamics

In experiment 4, we examine the importance of ocean dynamics by repeating the control run, except that now wind stress, which drives the equations of motion, is set to its annual average. Figure 9b shows that the effects of these processes are confined to two regions, the waters off northwest Africa and the band of latitudes between 15°S and 2°N. The easiest to understand is the SST cycle off northwest Africa. There, maximum SST occurs when the thermocline is deepest, and both occur when the southward component of the wind stress is weakest. The weakening of southward winds in August reduces coastal upwelling and allows surface heating to warm the mixed layer (Figure 10). These results are consistent with observations during the JOINT-I coastal ocean observation program of the mid-1970s [*Smith*, 1980].

Near the equator, SST is strongly controlled by upwelling across the bottom of the surface mixed layer due to divergence in either the zonal or meridional direction [*Weingartner and Weisberg*, 1991a, b; *Verstraete*, 1992]. Analysis of the motion and temperature fields suggests that in the western basin (west of 30°W) the weak annual change of SST is mainly produced by the annual variation in the meridional-vertical circulation. When the easterly component of the trade winds intensifies in May, upwelling strengthens because of the increasing meridional Ekman divergence. As more cold water is brought into the surface mixed layer, SST decreases until September, when maximum upwelling occurs. In contrast, the eastern equatorial Atlantic (east of 5°W) is a region of strong annually varying zonal divergence of the zonal surface currents (*Hastenrath and Merle* [1987] came to a different conclusion). The zonal mass divergence is compensated for by some convergence of mass in the meridional direction and by upwelling. The latter process is mainly responsible for cooling the mixed layer in boreal summer.

The relative importance of Ekman divergence and equatorward advection of cold water is examined in two additional experiments, in which the zonal (experiment 5) or meridional (experiment 6) components of the wind are replaced with their annual averages. The results, shown in Figures 11 and 12, confirm that annual variations in zonal stress are responsible for more than 30% of the annual cycle of SST along the equator. South of the equator, the amplitude of the zonal component of wind stress decreases to less than 0.05 N/m^2. *Hirst and Hastenrath* [1983] have suggested that some of the annual cycle of SST between 10°S and 0° is forced remotely by winds in the western basin. We examine this possibility in experiment 7, replacing the winds west of 28°W with their climatological annual average (Figure 13). The results indicate that only 25% of the annual cycle in this region results from wind variations in the western basin. The remainder of the annual cycle in this southern band of latitudes is due to (1) coastal upwelling associated with strengthening northward winds in northern summer, (2) zonal wind effects east of 28°W, and (3) the surface heat flux variations discussed earlier.

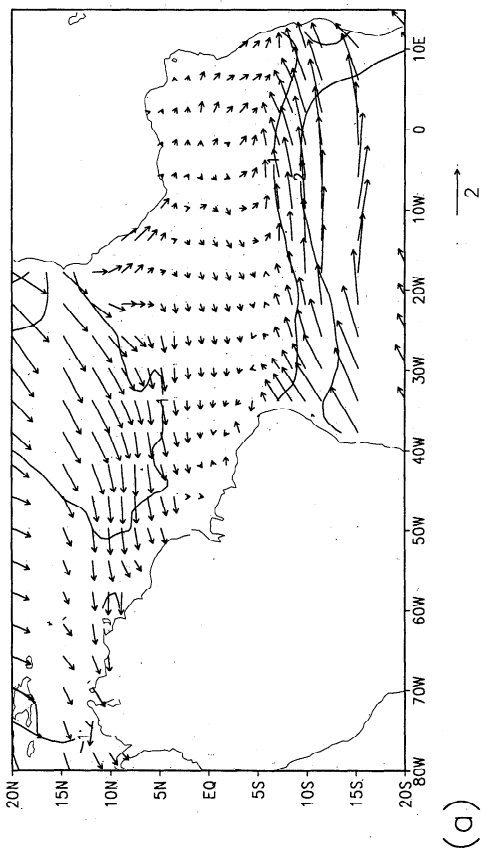

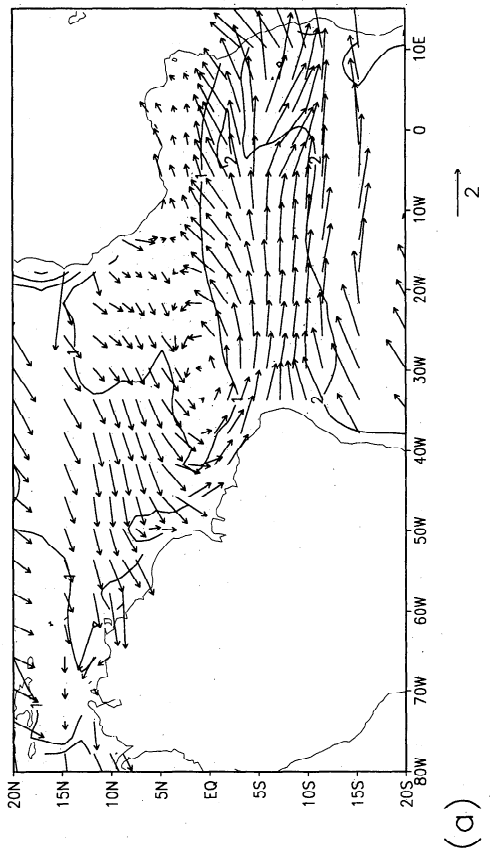

Figure 8. Annual cycle of SST from experiment 3 in which the humidity-induced variations in latent heating are introduced. An arrow that is pointing straight up indicates maximum occurs in January. Phase increases clockwise. Figure 8a shows amplitude and phase, and Figure 8b shows amplitude and phase of the difference between control run SST and experiment 3 SST. The difference may be interpreted as minus one times the contribution to the annual cycle of SST from latent heating variations due to wind variations. Contour intervals are 1°C and 0.25°C.

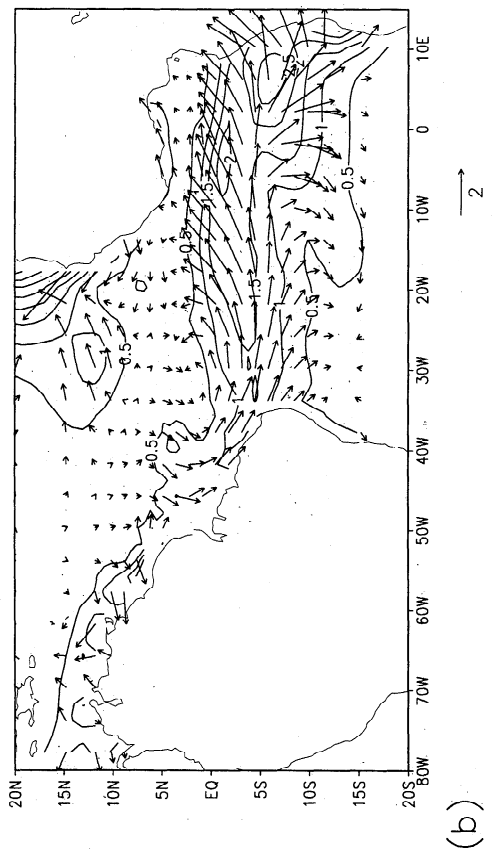

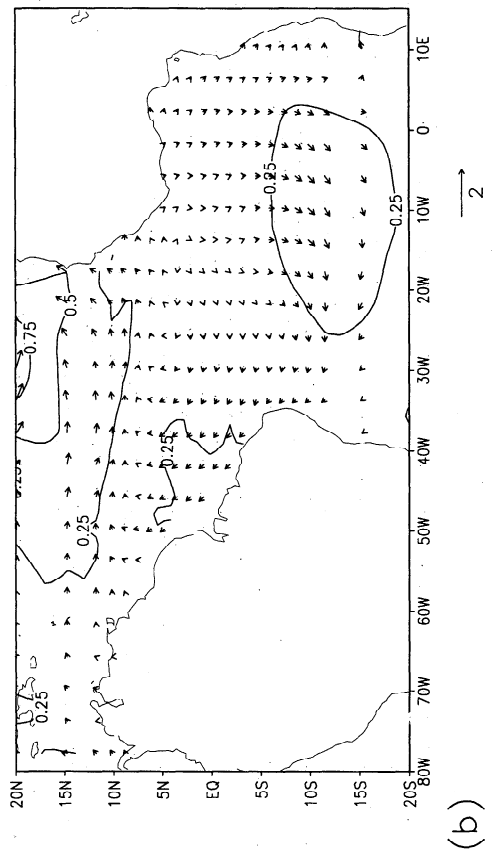

Figure 9. Annual cycle of SST from Expt. 4 in which wind stress is replaced with its annual average when it enters the equations of motion. An arrow that is pointing straight up indicates maximum occurs in January. Phase increases clockwise. Figure 9a shows amplitude and phase, and Figure 9b shows amplitude and phase of the difference between control run SST and experiment 4 SST. The difference may be interpreted as the contribution to the annual cycle of SST from dynamical effects variations. Contour intervals are 1°C and 0.5°C.

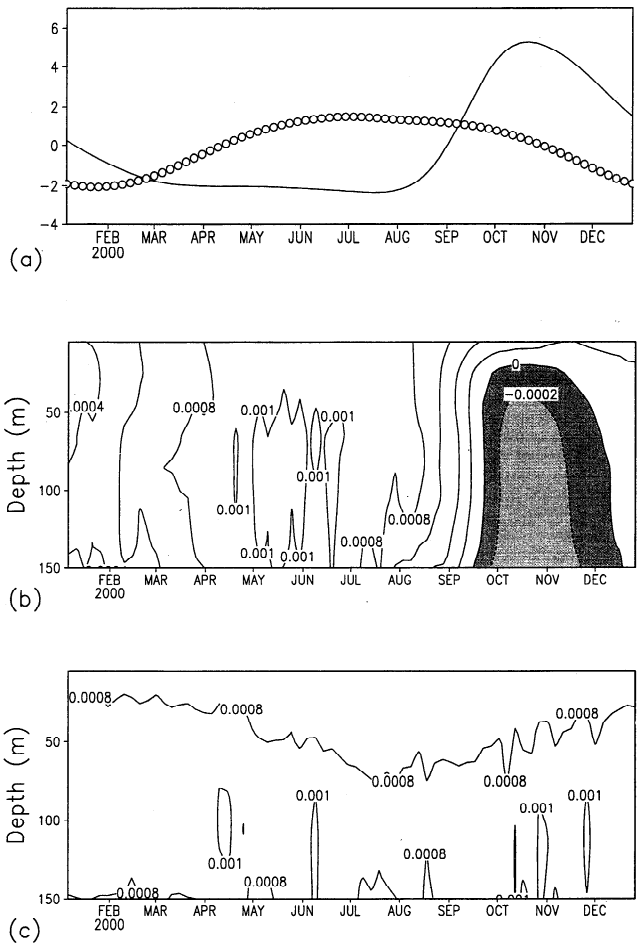

Figure 10. Contribution of dynamics to upwelling off northwest Africa, showing (a) SST anomaly from annual average for the control run (solid) and experiment 4 (open circles) at 20°N, 18°W, (b) vertical velocity with depth for control, and (c) vertical velocity with depth from experiment 4. Contour intervals are 0.0002 cm/s.

4. Summary

We examine the oceanic response to seasonally varying atmospheric forcing in the tropical Atlantic Ocean through a series of experiments with a general circulation model. We begin by examining its response to changes in the specified external forcing, including solar radiation, latent heating, and wind stress. In each case the simulated ocean response is compared to a control run forced by seasonally varying winds in which all forcing terms are included. In our analysis, we divide the response into the fraction due to surface heating processes and the remainder due to dynamical effects (either by altering advection or by changing the nature of heat flux across the base of the thermocline). The results are summarized in Figure 14.

The effect of surface heat flux on SST consists of two parts. Heat flux influences SST directly by warming the mixed layer and indirectly by modulating mixed layer depth and changing the size of the density discontinuity at the base of the mixed layer, which in turn, alters the rate of mixing. In three experiments we find the following.

1. Solar heating is most important south of 5°S and north of 10°N. At 20°S, solar heating induces a 2.4°C amplitude variation, while at 20°N, solar heating induces a smaller 1.2°C amplitude variation. Near the equator the amplitude directly due to solar heating reduces to 0.3°C and is mainly the result of annual variations in cloudiness in the eastern basin.

2. The most important factor in determining annual variations in latent heating is its dependence on surface wind speed. Latent heating is most important in the region 8°N–12°N, 50°W–25°W, where wind speed varies strongly seasonally. The dominance of latent heating in this region leads to the counterintuitive result that maximum SST occurs in the season when the thermocline is shallowest.

We examine the importance of ocean dynamics in several experiments modifying surface wind stress as it enters the equations of motion. Dynamics-induced changes in SST are mainly confined to two regions: the waters near northwest Africa and the band of latitudes 15°S–2°N. Within these regions we find the following.

1. Strong SST variations off northwest Africa are confined within a few hundred kilometers of the coast. Experiment 6 shows that they result from coastal upwelling during the winter months, when the northeast trade winds intensify.

2. SST variations along the equator are regulated primarily by ocean dynamics. East of 20°W, boreal summer cooling is the result of zonal divergence of mass, which is compensated for by upwelling and convergence in the meridional direction. In the western basin, SST variations are controlled by the annual variation in the meridional-vertical circulation. Meridional Ekman divergence causes upwelling, cooling the ocean surface. Although the annual variations of winds are stronger in the western basin than the eastern basin, the annual variations of SST are stronger in the eastern basin because of the shallow thermocline in that region.

3. SST variations in the region extending from the equator southward result from a combination of local and remote effects. The strongest factor in determining SST variations near the coast of southwest Africa is the perturbation of the depth of the thermocline resulting from remote equatorial effects that propagate southward along the coast. Thus the annual cycle of SST there is in phase with variations in cross-shelf oriented zonal winds rather than along shelf oriented meridional winds.

It has been proposed that the annual cycle of winds and temperature in the equatorial Pacific result from air-sea interaction. According to *Mitchell and Wallace* [1992], monsoonal winds near the coast of South America induce upwelling in the southeastern basin during boreal summer. The cool ocean temperatures propagate westward because of their influence on the trade winds. In the Atlantic, SSTs along the coast of southern Africa are controlled by several factors, among which monsoonal winds are not the most important. However, once cold water appears along the coast of southern Africa in June, the westward spread of the cold tongue may occur by processes similar to those proposed for the Pacific.

The model used in these experiments does have several deficiencies that should be mentioned. Throughout the basin, the mixed layer is unrealistically shallow, suggesting that mixed layer processes are being modeled imperfectly. The problem is particularly striking in the Gulf of Guinea. Our mixing scheme is based on mixing length theory, in which the mixing length varies with bulk Richardson number. This is done to model the effects of shear instability. Improvements in mixed layer physics, including the introduction of a higher order mixing scheme

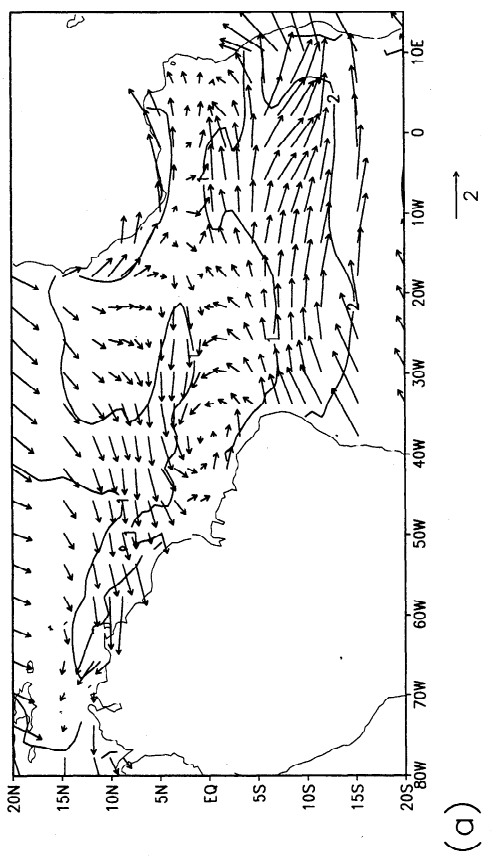

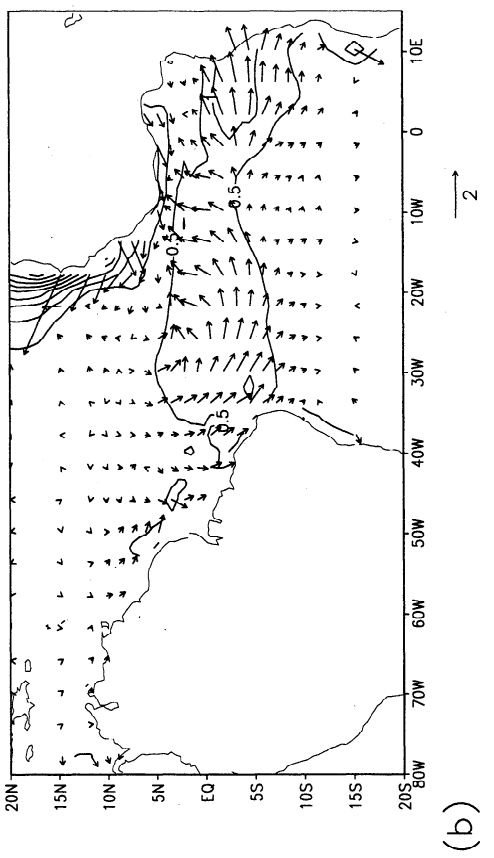

Figure 12. Annual cycle of SST from experiment 6 in which only the meridional component of wind stress is replaced with its annual average when it enters the equations of motion. An arrow that is pointing straight up indicates maximum occurs in January. Phase increases clockwise. Figure 12a shows amplitude and phase, and Figure 12b shows amplitude and phase of the difference between control run SST and experiment 6 SST. Contour intervals are 1°C and 0.5°C.

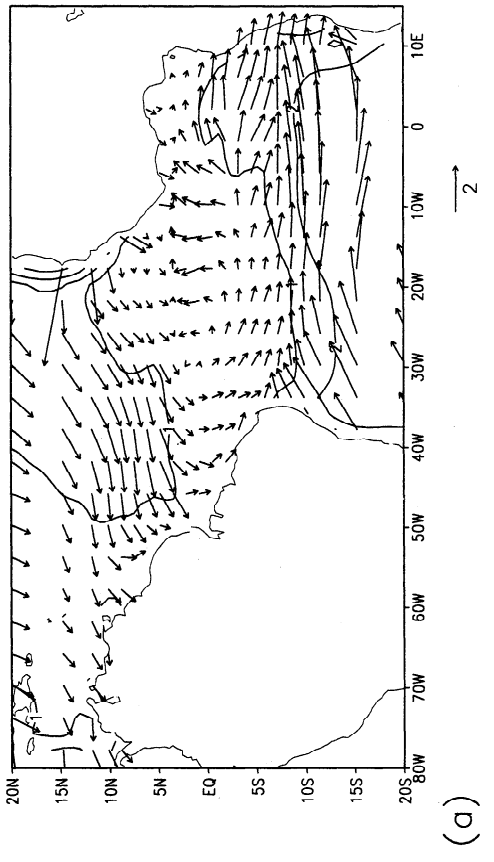

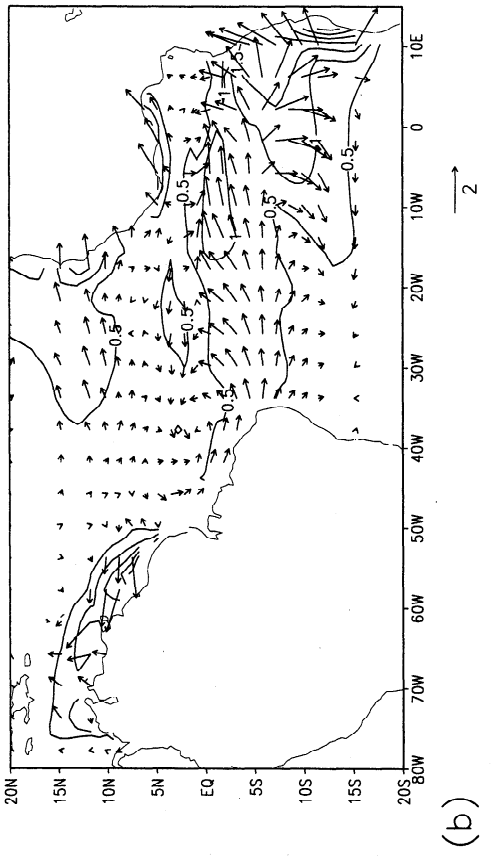

Figure 11. Annual cycle of SST from experiment 5, in which only the zonal component of wind stress is replaced with its annual average when it enters the equations of motion. An arrow that is pointing straight up indicates maximum occurs in January. Phase increases clockwise. Figure 11a shows amplitude and phase, and Figure 11b shows amplitude and phase of the difference between control run SST and experiment 5 SST. Contour intervals are 1°C and 0.5°C.

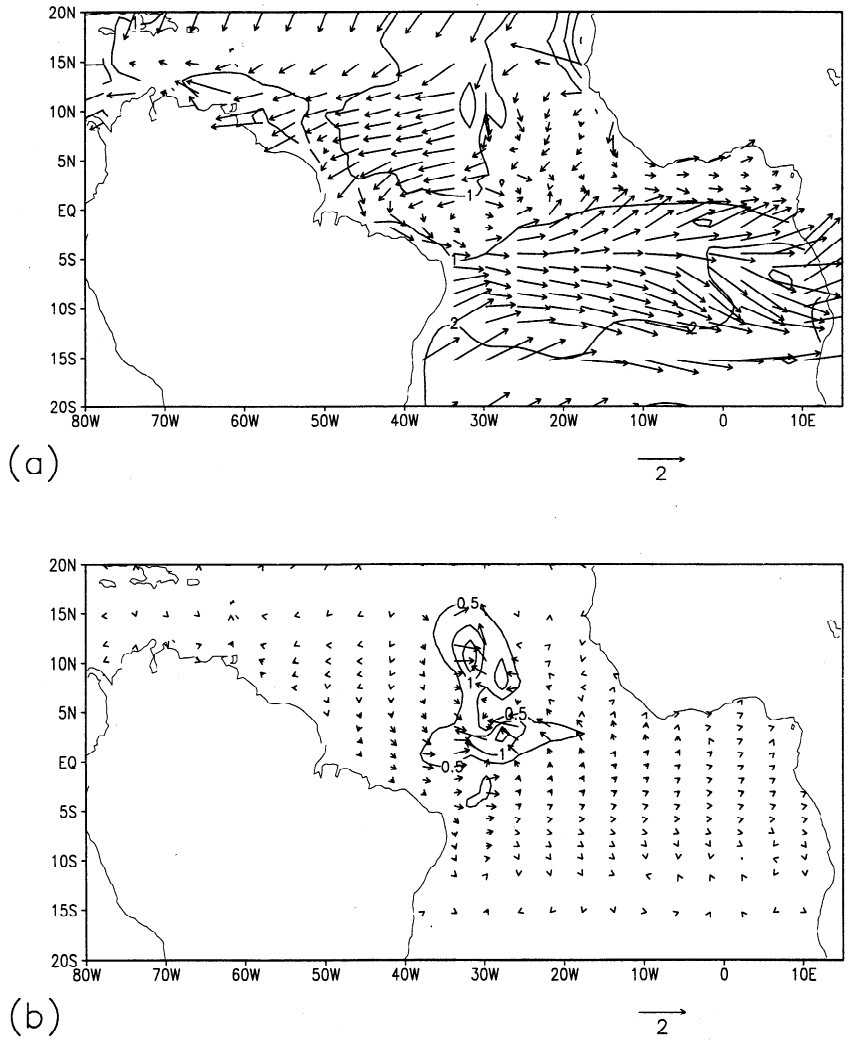

Figure 13. Annual cycle of SST from experiment 7, in which only the zonal component of wind stress west of 30°W is replaced with its annual average when it enters the equations of motion. An arrow that is pointing straight up indicates maximum occurs in January. Phase increases clockwise. Figure 13a shows amplitude and phase, and Figure 13b shows amplitude and phase of the difference between control run SST and experiment 7 SST. Contour intervals are 1°C and 0.5°C.

[*Blanke and Delecluse*, 1993] may be required. Additionally, it is worth emphasizing that seasonal winds have been used throughout these experiments. Although the observed winds in the tropical Atlantic are primarily seasonal in character, intraseasonal and interannual variations of the winds do occur that may contribute in important ways to the seasonal cycle of SST because of the nonlinear nature of the equations governing SST.

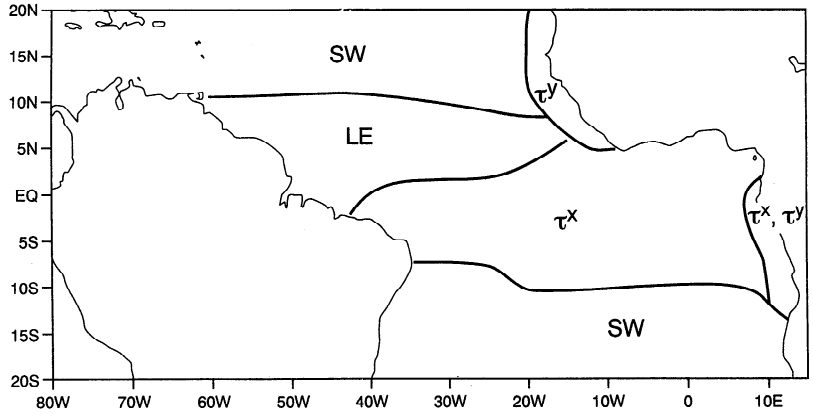

Figure 14. Schematic diagram indicating the dominant terms controlling the annual cycle of SST.

Acknowledgment. Support for this research has been provided by the National Science Foundation under grant OCE9416894.

References

Blanke, B., and P. Delecluse, Variability of the tropical Atlantic Ocean simulated by a general circulation model with two different mixed-layer physics, *J. Phys. Oceanogr.*, *23*, 1363–1388, 1993.

Blumenthal, M. B., Effects of west African air humidity on Atlantic sea surface temperature, in *Greenhouse Effect, Sea Level and Drought*, edited by P. R. Paepe, R. W. Fairbridge, and S. Jelgersma, pp. 21–40, Kluwer Acad., Norwell, Mass., 1990.

Budyko, M. I., *Climate and Life, Int. Geophys. Ser.*, vol. 18, 508 pp., Academic, San Diego, Calif., 1974.

Busalacchi, A. J., and J. Picaut, Seasonal variability from a model of the tropical Atlantic Ocean, *J. Phys. Oceanogr.*, *13*, 1564–1588, 1983.

Carton, J. A., and E. C. Hackert, Assimilation analysis of tropical Atlantic circulation during 1983–4, *J. Phys. Oceanogr.*, *20*, 1150–1165, 1990.

da Silva, A. M., C. C. Young, and S. Levitus, *Atlas of Surface Marine Data 1994*, vol. 1, *Algorithms and Procedures*, *NOAA Atlas Ser.*, U.S. Gov. Print. Off., Washington, D. C., 1994.

du Penhoat, Y., and A. M. Triguier, The linear seasonal response of the tropical Atlantic Ocean, *J. Phys. Oceanogr.*, *15*, 316–329, 1985.

Garzoli, S. L., and E. J. Katz, The forced annual reversal of the Atlantic North Equatorial Countercurrent, *J. Phys. Oceanogr.*, *13*, 2082–2090, 1983.

Giese, B. S., and D. R. Cayan, Surface heat flux parameterizations and tropical Pacific sea surface temperature simulations, *J. Geophys. Res.*, *98*, 6979–6989, 1993.

Harrison, D. E., Equatorial sea surface temperature sensitivity to net surface heat flux: Some ocean circulation model results, *J. Clim.*, *4*, 539–549, 1991.

Hastenrath, S., and J. Merle, Annual cycle of subsurface thermal structure in the tropical Atlantic Ocean, *J. Phys. Oceanogr.*, *17*, 1518–1538, 1987.

Hayes, S. P., P. Chang, and M. J. McPhaden, Variability of the sea surface temperature in the eastern equatorial Pacific Ocean, *J. Phys. Oceanogr.*, *96*, 10,553–10,566, 1991.

Hirst, A. C., and S. Hastenrath, Atmosphere-ocean mechanism of climate anomalies in the Angola–tropical Atlantic sectors, *J. Phys. Oceanogr.*, *13*, 1146–1157, 1983.

Horel, J. D., A rotated principal component analysis of the interannual variability of the northern hemisphere 500 mb height field, *Mon. Weather Rev.*, *109*, 2080–2092, 1981.

Koberle, C., and S. G. H. Philander, On the processes that control seasonal variations of sea surface temperatures in the tropical Pacific Ocean, *Tellus*, *46A*, 481–496, 1994.

Kraus, E. B. (ed.), *Modeling and Prediction of the Upper Layers of the Ocean*, Pergamon, Tarrytown, N. Y., 1997.

Liu, W. T., and C. Gautier, Thermal forcing on the tropical Pacific from satellite data, *J. Geophys. Res.*, *95*, 13,209–13,217, 1990.

Merle, J., and S. Arnault, Seasonal variability of the surface dynamic topography in the tropical Atlantic Ocean, *43*, 267–288, 1985.

Mitchell, T. P., and J. M. Wallace, The annual cycle in equatorial convection and sea surface temperature, *J. Clim.*, *5*, 1140–1156, 1992.

Nigam, S., and Y. Chao, On the evolution-dynamics of tropical ocean-atmosphere annual-cycle variability, *J. Clim.*, in press, 1997.

Pacanowski, R., and S. G. H. Philander, Parameterization of vertical mixing in numerical models of tropical oceans, *J. Phys. Oceanogr.*, *11*, 1443–1451, 1981.

Philander, S. G. H., and R. C. Pacanowski, A model of the seasonal cycle in the tropical Atlantic Ocean, *J. Geophys. Res.*, *91*, 14,192–14,206, 1986.

Seager, R., S. E. Zebiak, and M. A. Cane, A model of the tropical Pacific sea surface temperature climatology, *J. Geophys. Res.*, *93*, 1265–1280, 1988.

Seager, R., M. B. Blumenthal, and Y. Kushnir, An advective atmospheric mixed layer model for ocean modeling purposes: Global simulation of surface heat fluxes, *J. Clim.*, *8*, 1951–1964, 1995.

Smith, R. L., A comparison of the structure and variability of the flow field in three coastal upwelling regions: Oregon, northwest Africa, and Peru, in *Coastal Upwelling*, *Coastal Estuarine Sci.*, vol. 1, edited by F. A. Richards, pp. 107–117, AGU, Washington, D. C., 1980.

Verstraete, J.-M., The seasonal upwellings in the Gulf of Guinea, *Progr. Oceanogr.*, *29*, 1–60, 1992.

Wang, B., On the annual cycle in the equatorial Pacific cold tongue, *J. Clim.*, *7*, 1926–1942, 1994.

Weingartner, T. J., and R. H. Weisberg, On the annual cycle of equatorial upwelling in the central Atlantic Ocean, *J. Phys. Oceanogr.*, *21*, 68–82, 1991a.

Weingartner, T. J., and R. H. Weisberg, A description of the annual cycle in sea surface temperature and upper ocean heat in the equatorial Atlantic, *J. Phys. Oceanogr.*, *21*, 84–96, 1991b.

Wyrtki, K., An estimate of equatorial upwelling in the Pacific, *J. Phys. Oceanogr.*, *11*, 1205–1214, 1981.

J. A. Carton, Department of Meteorology, University of Maryland, College Park, MD 20742.

Z. Zhou, Atlantic Oceanographic Marine Laboratory, NOAA, 4301 Rickenbacker Causeway, Miami, FL 33149.

(Received September 30, 1996; revised June 9, 1997; accepted July 30, 1997.)